

Photocatalytic reduction and scavenging of Hg(II) over templated-dewetted Au on TiO₂ nanotubes

Davide Spanu^{a,b}, Alessandro Bestetti^a, Helga Hildebrand^b, Patrik Schmuki^{b,c}, Marco Altomare^b and Sandro Recchia^{a,*}

^a Department of Science and High Technology, University of Insubria, via Valleggio 11, 22100 Como, Italy

^b Department of Materials Science and Engineering WW4-LKO, University of Erlangen-Nuremberg, Martensstrasse 7, D-91058 Erlangen, Germany

^c Chemistry Department, Faculty of Sciences, King Abdulaziz University, 80203 Jeddah, Saudi Arabia Kingdom

* Corresponding author. Email: sandro.recchia@uninsubria.it

Link to the published article:

<https://pubs.rsc.org/en/content/articlehtml/2018/pp/c8pp00424b>

Abstract

Gold-decorated TiO₂ nanotubes were used for the photocatalytic abatement of Hg(II) in aqueous solutions. The presence of dewetted Au nanoparticles induces a strong enhancement of photocatalytic reduction and scavenging performances, with respect to naked TiO₂. In the presence of chlorides, a massive formation of Hg₂Cl₂ nanowires, produced from Au nanoparticles, was observed using highly Au loaded photocatalysts to treat a 10 ppm Hg(II) solution. EDS and XPS confirmed the nature of the photo-produced nanowires. In the absence of chlorides and/or at lower Hg(II) starting concentrations, the scavenging of mercury proceeds through the formation of Hg-Au amalgams. Solar light driven Hg(II) abatements up to 90% were observed after 24h. ICP-MS analysis revealed that the removed Hg(II) is accumulated on the photocatalyst surface. Regeneration of Hg-loaded exhaust photocatalysts was easily performed by anodic stripping of Hg(0) and Hg(I) to Hg(II). After four catalytic-regeneration cycles only a 10% decrease of activity was observed.

Introduction

Pollution of water with mercury and its compounds has received increasing attention due to its toxic and bioaccumulative properties.¹⁻⁵ High levels of Hg(II) can be found in industrial wastewaters coming from activities which extensively use mercury, such as chlorine-alkali, petrochemical, metallurgical, paint and electrical industry.^{1,6} Inorganic Hg(II) in water bodies can be transformed by a large number of anaerobic bacteria to methylmercury, which is a well-known neurotoxin. This compound is strongly held to fish protein when absorbed through the gills or when contaminated food sources are eaten. In some cases, methylmercury levels in carnivorous fish can be biomagnified up to a million times higher concentration levels than in the surrounding water.^{5,7,8} Thus, the alkylation process of Hg(II) poses a serious health risk to humans and fauna through the aquatic food chain: even if Hg(II) is present at very low concentration, few $\mu\text{g L}^{-1}$ of Hg(II) could already lead to a significant mercury alkylation).

For these reasons, very restrictive worldwide regulations have been enacted with the goal of reducing mercury emissions into surface water bodies.⁹ Nonetheless, the disposal of mercury currently represents a major environmental concern, and the development of new technologies for a green and efficient removal of Hg(II) from water is still a challenge.

Mercury can be successfully removed from highly concentrated aqueous solutions by membrane filtration, precipitation, ion exchange, adsorption and other methods.¹⁰⁻¹² However, these techniques become less efficient and more expensive with mercury concentration lower than 100 ppm.¹²⁻¹⁴ This represents a great limitation because even in the presence of relatively low Hg concentrations high abatement rates are a fundamental prerequisite for a successful and viable removal technique.

A “green approach” that is emerging as one of the most promising method for mercury removal is the photocatalytic reduction of Hg(II), which combines simplicity of operation and

could reach high performances even when treating feedstock with low mercury concentrations.^{14–20}

Photocatalysis is based on the irradiation, with a proper light source, of a semiconductor, usually a metal oxide (e.g. TiO_2 , Fe_2O_3 , WO_3), which induces the promotion of electrons from the valence band (VB) to the conduction band (CB) leaving holes in the CB. The photo-generated holes and electrons can recombine (in the bulk or at the semiconductor surface) or, more preferably, can react with adsorbed species or with species in the environment to cause redox reactions.

Various metal oxide semiconductors have been explored as photocatalysts, and their field of application has been expanded in the recent years.^{21–23}

Among these materials titanium dioxide (TiO_2) is undoubtedly considered one of the best photocatalytic material for a wide range of processes.^{21,24–26} Several advantages of TiO_2 are its non-toxicity, low-cost, long-term stability, and corrosion and photo-corrosion stability.

In particular, nanostructured TiO_2 , such as TiO_2 nanotubes (NTs),^{25,27–30} having a one-dimensional (1D) morphology and a large specific surface area, exhibit a strongly enhanced photo(electro)chemical performance due to directional charge transport, together with a beneficial diffusion and adsorption geometry.^{31–33}

TiO_2 is n-type semiconductor with a band gap of 3.00–3.20 eV, depending on its crystallographic structure. TiO_2 can be easily synthesized in two main crystalline forms: the most common ones are rutile (tetragonal, with a band gap of around 3.00 eV) and anatase (tetragonal, with a band gap of around 3.20 eV).^{34,35}

In aqueous solution, the species that in principle can be oxidized by holes photo-generated in TiO_2 are water, hydroxyl ions, and, if present, organic compounds. Instead, promoted electrons can reduce oxygen (to produce superoxide radicals) or metallic ions – this given that

the potential of the conduction band (CB) edge of the semiconductor is more negative than the reduction potential of the $M^{n+}/M^{(n-m)+}$ couple.³⁶ The knowledge of the reduction potential of the metal ions and the level of CB edge of the semiconductor is fundamental to predict the thermodynamic feasibility of the reduction: the higher the difference between these values, the higher the tendency towards reduction of metallic ions.³⁷ In the case of Hg(II)/Hg(0) and the CB edge of TiO₂, the potentials have been reported to “seat” at 0.851 V (vs NHE)³⁸ and ≈ -0.50 V (at pH 7 vs NHE),³⁹ respectively – that is, it is thermodynamically possible to photo-reduce Hg(II) at the TiO₂ surface.

The photocatalytic reduction of Hg(II) over powdered TiO₂ has been previously reported in several works.^{14–20} First attempts to photo-reduce Hg(II) on powdered TiO₂ photocatalysts were made by using commercial Degussa P25 and Hombikat UV100 (100% anatase) under UV light illumination.^{16–18} Few years later Lenzi et al.¹⁹ tried to improve the adsorption and photocatalytic performance by preparing via sol-gel and impregnation a Ag/TiO₂ powder with higher specific surface area.

To the best of our knowledge, the utilization of titania in a supported form (WO₃-decorated TiO₂ nanotubes) was reported only by Lee et al.,¹⁴ who obtained promising mercury abatement results; $\sim 76\%$ of the initial Hg(II) content was removed in 2 hours, under illumination of a UV-B (280-315 nm, 96 W) germicidal lamp. However the utilization of such a powerful light source, and the lack of data on the total irradiance that was used, makes it difficult to compare the results with previous and future photocatalysts.

In any case, no data about the exploitation of the potential beneficial effects of the presence of gold over TiO₂ are reported in the literature. In principle the presence of gold should enhance the photocatalytic performances of TiO₂ towards Hg(II) abatement by: i) increasing the charge

carriers separation and enhancing the electron transport to the TiO₂/electrolyte interface; ii) improving the Hg scavenging properties, through the in-situ formation of Hg-Au amalgams.

In this work we investigate for the first time, the performance of Au nanoparticles (NPs) modified TiO₂ nanotubes towards the solar light-driven Hg(II) photocatalytic reduction. More in detail, we found that the Hg accumulation capabilities of our Au/TiO₂ systems are unexpectedly high, with two main different mechanisms operating at higher or lower Hg concentrations. The influence of the presence of different amounts of gold and the regeneration/recycling ability of the photocatalysts were also explored.

Experimental

Preparation procedure of Au-TiO₂ NTs

Ti foils (Advent Research Materials, 0.125 mm thickness, 99.6+% purity) were degreased by sonicating in acetone, isopropanol, and deionized water and then were dried in a N₂ stream. The cleaned Ti foils were anodized to fabricate the highly ordered TiO₂ nanotube arrays at 100°C in a 3M HF solution in o-H₃PO₄ (Sigma- Aldrich). For this process, a two-electrode configuration was used, where the Ti foil (15 mm × 15 mm) was the working electrode and a Pt sheet was the counter electrode. The anodization was performed by applying a potential of 15 V (for 2 h) using a DC power supply (VLP 2403 Voltcraft). Subsequently, the TiO₂ nanotube arrays on Ti metal substrates were rinsed with ethanol and dried under N₂ stream.

After anodization and rinsing, an Au metal thin film was sputtered on the synthesized TiO₂ NTs layer by a plasma-sputtering machine (EM SCD 500, Leica) using a 99.999% pure Au target with an applied sputtering current of 16 mA and pressure of 10⁻² mbar of Ar. The amount of sputtered material was in-situ determined by an automated quartz crystal monitor, and is reported in this work as nominal thickness of the sputtered film. After sputtering, the samples

were annealed at 450°C in air to crystallize TiO₂ NTs and to induce dewetting (as described by Yoo et al.⁴⁰). Although other deposition techniques can be used to obtain Au-decorated nanotubes (see ref.⁴¹ as an example) we decided to use the templated-dewetting approach to obtain two morphologically different systems just changing the Au loading (i.e. just changing the sputtering time).

Characterization techniques

The morphology of photocatalytic material was studied using a XL30 Environmental Scanning Electron Microscopy (ESEM FEG Philips) at 20 kV under high and low vacuum conditions. Elemental analysis were performed with a silicon drifted EDS detector (EDAX element). High resolution SEM images were collected using a Hitachi S4800 FE-SEM.

XRD data were recorded on a Rigaku Miniflex system using Cu-K α radiation, 30 kV, 10 mA with step of 0.02° (2 θ) and a scanning speed of 2° min⁻¹.

XPS spectra were acquired using Al X-ray source. The XPS spectra were corrected in relation to the Ti2p signal at 458.5 eV. PHI MultiPak™ software and database were used for curve fitting analysis.

A Sun 2000 Solar Simulator (Abet Technologies, calibrated at 100 mW cm⁻²) equipped with an AM 1.5 G filter was used as the vertical light source: a totally reflecting mirror has been used to deflect the light beam and to carry out the experiments in a side-illumination configuration.

A three-electrode system connected to an Amel 2551 potentiostat equipped with a silver chloride reference electrode (Ag/AgCl/saturated KCl), and a Pt wire as counter electrode was used for the photoelectrochemical (PEC) characterization (cyclic voltammetry and chrono-amperometry).

All measurements were performed using a 250 mL quartz beaker, placed over a magnetic stirrer: 135 g of solution were used in each test to obtain a good light focus and a total immersion of the electrodes.

Photocatalytic Hg(II) reduction tests

The same quartz cell and solar simulator described for the characterization techniques were used to carry out Hg(II) photo-reduction tests. Ultrapure water (MilliQ 18.2 M Ω cm, 3ppb TOC) was used for the preparation of all solutions. Abatement tests were conducted in solutions containing: i) 2 mM phosphate buffer (pH 7.0, 630 μ S cm⁻¹) obtained by dilution of a concentrated 200 mM phosphate buffer, ii) 100 mM of NaCl (prepared by dissolution of solid NaCl, Sigma-Aldrich, \geq 98%).

The presence of Hg(II) in solution was ensured by the addition of a proper amount of a diluted solution obtained from the concentrated 1000 mg L⁻¹ Hg(II) solution, that was prepared by dissolving 338.4 mg of HgCl₂ (Carlo Erba, \geq 99.5%) in 250 mL ultrapure water. Total mercury concentration was determined on properly diluted samples that were collected during the photocatalytic experiment with a Thermo Scientific ICAP Q inductively coupled plasma mass spectrometer (ICP-MS). The Hg concentration was determined by monitoring the 202-Hg channel and using a He-collision cell in kinetic energy discrimination (KED) mode, following the standard conditions indicated by the factory. Both external standards (prepared by dilution from a 10 mg L⁻¹ Hg stock solution, Merck) and internal standards (10 ppb of Germanium added in each sample by dilution from a 1000 mg L⁻¹ Ge stock solution, Fluka TraceSELECT®) were employed for Hg quantification. In addition, 0.2 mol L⁻¹ of BrCl solution, prepared by dissolving 2.7 g of KBr (Sigma-Aldrich, \geq 99.0%) in 250 mL HCl (Fluka, > 30%, TraceSELECT®) and adding 3.8 g of KBrO₃ (Sigma-Aldrich, \geq 99.0%), were added to all

analyzed solutions with a 1:100 dilution, in order to minimize mercury memory effects in ICP-MS analysis.⁴²

Photoelectrochemical regeneration of Au-TiO₂ photocatalysts

The same quartz cell, three-electrode system and solar simulator described for the characterization techniques were used to carry out the PEC regeneration of Au-TiO₂ photocatalysts. After every Hg(II) abatement experiment, Au-TiO₂ NTs samples were dipped in a 100 mM KNO₃ (prepared by dissolving solid KNO₃, Sigma-Aldrich, $\geq 99.0\%$) solution and a positive +500 mV (vs. Ag/AgCl) potential was applied for 2 hours under stirring and front solar-irradiation. Cyclic voltammograms from -200 mV to +1000 mV (vs. Ag/AgCl) with a scan speed of 200 mV s⁻¹ were recorded in this solution under permanent illumination conditions. The resulting solutions were analyzed in view of their composition with ICP-MS as described for the samples collected for photocatalytic reduction.

Results and discussion

Fig. 1a shows the morphology of the top and cross-sectional view (see inset in Fig. 1a) of the highly-ordered TiO_2 NTs employed in this work, which are anodically grown on Ti metal foils in a hot, concentrated $\text{H}_3\text{PO}_4/\text{HF}$ electrolyte.⁴⁰ These well-defined nanostructures exhibit a nearly ideal hexagonal packing and each tube has an average internal diameter of ~ 90 nm and a length of ~ 200 nm.

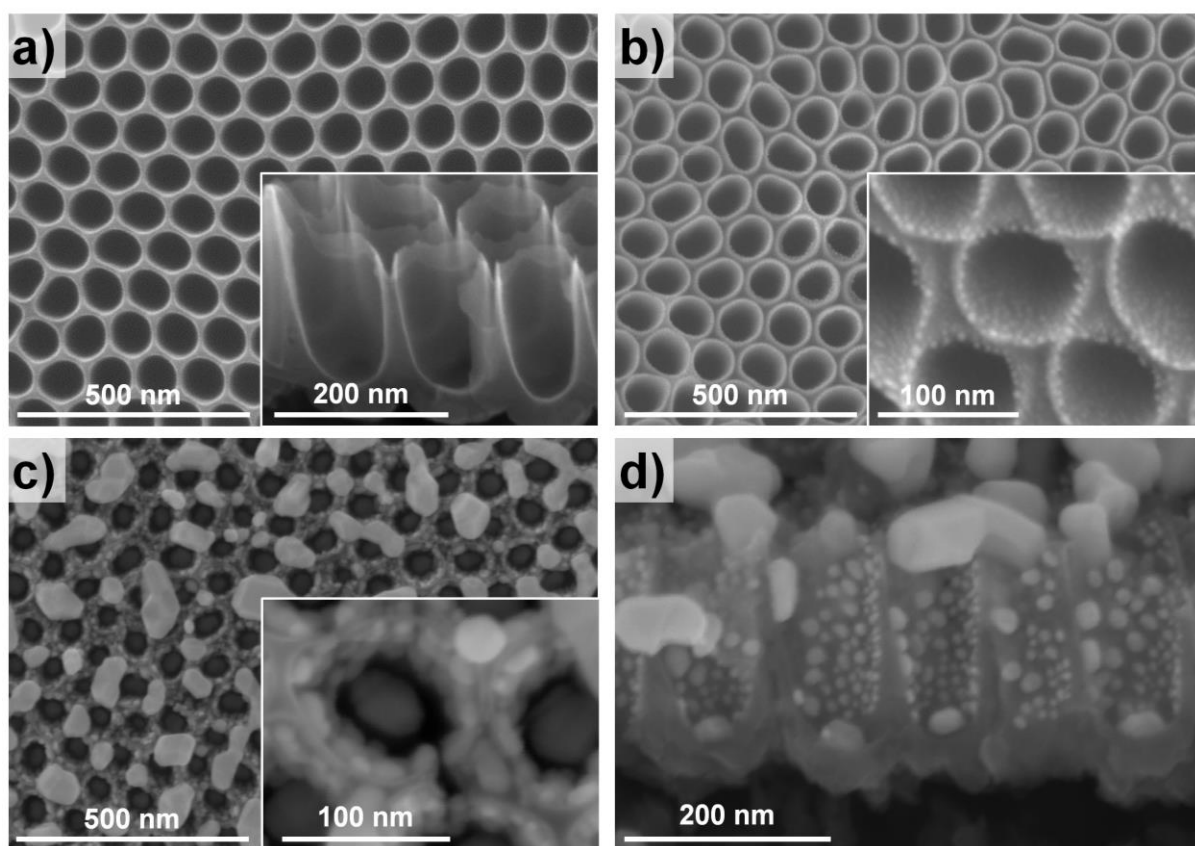


Fig. 1. (a-d) SEM images of TiO_2 structures employed in this work: (a) top view of pristine TiO_2 nanotubes. Inset: cross-sectional view of pristine TiO_2 ; (b) TiO_2 NTs coated with a sputtered 1 nm-thick Au film after dewetting (1Au- TiO_2). Inset: magnified top view image of 1Au- TiO_2 ; (c) TiO_2 NTs coated with a sputtered 20 nm-thick Au film after dewetting (20Au- TiO_2). Inset: magnified top view image of 20Au- TiO_2 ; (d) cross-sectional view of 20Au- TiO_2

As reported in previous work these NT arrays can be decorated with nanoscopic precision by sputter-deposition of a thin metal film (Au in this work) followed by a proper thermal treatment that induces both the crystallization of TiO_2 and the solid-state templated-dewetting

of the metal.^{40,43–48} Images of TiO₂ NTs coated with a nominally 1 nm-thick (1Au-TiO₂) and 20 nm-thick (20Au-TiO₂) Au layers after a heat treatment (i.e. after dewetting) are reported in Fig. 1b and 1c-d, respectively. Thermal dewetting of metal thin films occurs at the solid-state: the temperature of the thermal treatment is far below the melting point of Au. Essentially, the driving force for dewetting is related to the minimization of: i) the free surface energy of the oxide surface (TiO₂), ii) the free surface energy of the metal layer (Au) and iii) the interfacial energy of the metal/substrate system (Au/TiO₂).^{45,49}

For the sake of comparison, Fig. S1a and S1b show the SEM images recorded prior dewetting for 1Au-TiO₂ and 20Au-TiO₂, respectively: in the case of the 20 nm deposition a strong difference between pristine and dewetted samples can be observed, while for the 1 nm specimen no significant differences can be appreciated, as for this sample dewetting occurs at nearly room temperature (so thin layers require low energy input to dewet).⁴⁵ Analogous structures (same anodization conditions, thermal treatment and sputtered metal) were prepared and characterized (XRD, XPS and hydrogen evolution capability under UV irradiation) in a previous work.⁴⁰

In this work, Au-TiO₂ systems were assessed in view of their photocatalytic Hg(II) reduction performance under solar light simulated irradiation. Both 1Au-TiO₂ and 20Au-TiO₂ were tested over solutions buffered at pH 7.0 (see experimental section), having two markedly different Hg starting concentrations.

Fig. 2 shows the results of the photocatalytic abatement tests of both 1Au-TiO₂ and 20Au-TiO₂ systems, carried out with solutions having a starting Hg concentration of 10 ppm (Fig. 2a) or 500 ppb (Fig. 2b).

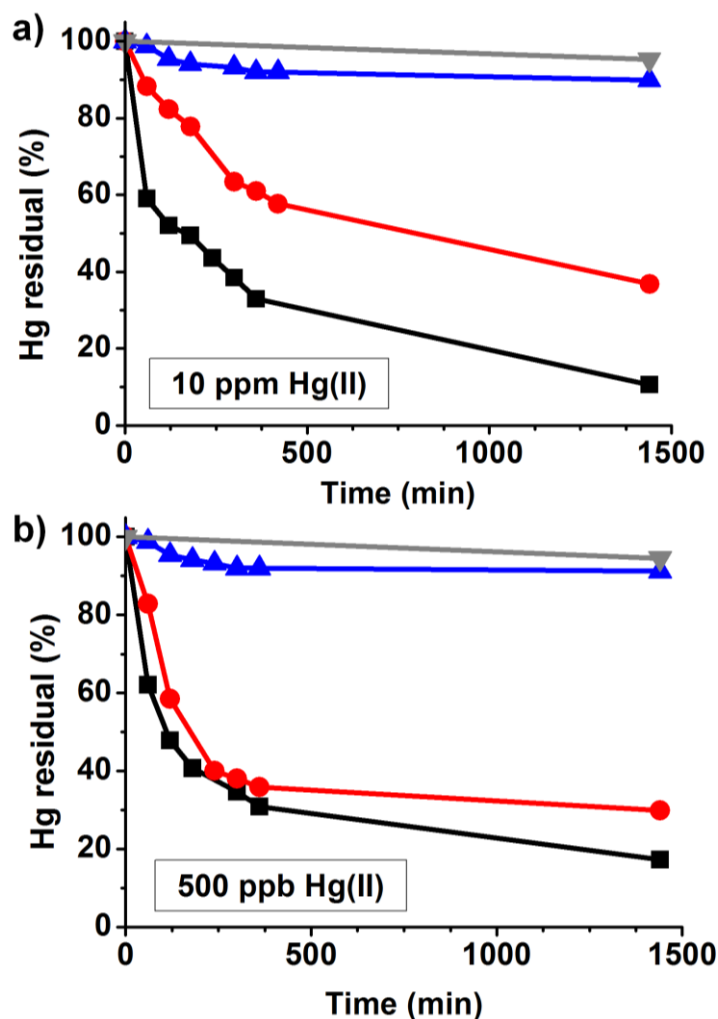


Fig. 2. (a-b) Hg(II) concentration trends during photocatalytic reduction using 20Au-TiO₂ (black), 1Au-TiO₂ (red), TiO₂ (blue) and 20Au-TiO₂ in dark condition (grey) at pH 7.0 in presence of chloride with different starting Hg(II) concentrations: (a) 10 ppm and (b) 500 ppb.

The reported Hg reduction profiles are surely correlated to photo-activated processes, as no significant Hg abatement is observed in the dark. Moreover, a comparison of the abatement profiles obtained for naked TiO₂ and for both Au-TiO₂ systems strongly indicates that gold decoration is fundamental to obtain high photocatalytic Hg(II) reduction (removal) rates. As a preliminary consideration, the strong promotion effect caused by the presence of Au NPs might be ascribed to: i) the improvement of the electron transfer to reactants provided by Au NPs (localized Schottky-junctions);²⁸ ii) the strong interaction between Hg and Au that can lead to the formation of nano-alloys (“nano-amalgams”, if Hg(II) is completely reduced to Hg(0) and

incorporated in the Au NPs). In particular, the best photocatalytic performance was obtained with the most Au-loaded photocatalyst (20Au-TiO₂), which is able to reduce up to ~ 90 % of Hg(II) after 24 hours, almost independently of the starting Hg(II) concentration. Instead, 1Au-TiO₂ exhibits a certain sensitivity to the mercury starting concentration: the higher the Hg(II) starting concentration, the lower the photocatalytic efficiency.

During the abatement of the 10ppm Hg solution the formation of a compact white-grayish layer was macroscopically observed on 20Au-TiO₂. Surprisingly, SEM images recorded on this specimen at the end of the abatement test revealed that the catalysts' surface is homogeneously covered by nano filaments, having a ~ 100 nm mean width and length of some tens of microns (Fig. 3a). The formation of such nanofibers is very reproducible, as it was always observed with different 20Au-TiO₂ specimens and even after each regeneration and recycling test (discussed below). No detachment of the compact layer of such nanowires from the catalyst surface was observed even after 24h. EDS analysis carried out on several of these filaments revealed that they are mainly composed by Hg and Cl, with an approximate Hg/Cl atomic ratio of 1.1. It therefore reasonable to suggest the formation of insoluble Hg₂Cl₂ filaments, which is possible due to the presence of NaCl in the aqueous medium (additional characterization data to support the formation of Hg₂Cl₂ are shown below).

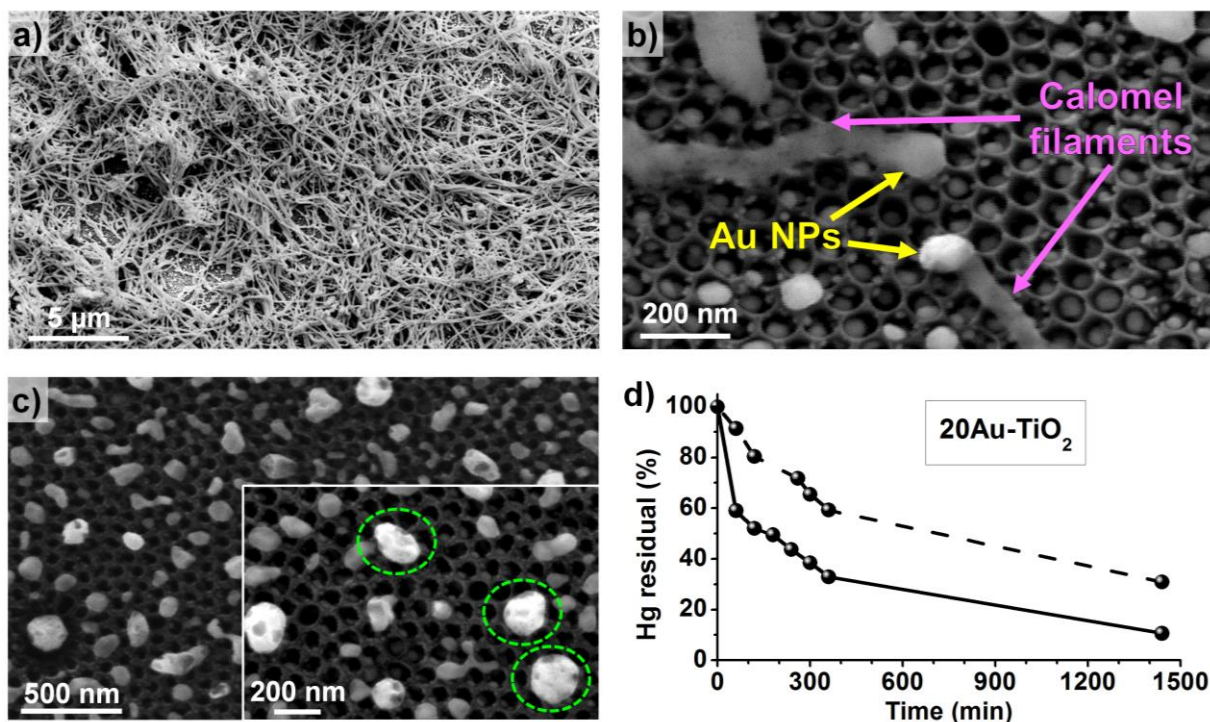


Fig. 3. (a-b) SEM images of 20Au-TiO₂ recorded after (a) 24 hours and (b) 30 minutes long photocatalytic reduction of 10 ppm of Hg(II) in presence of chloride. (c) 20Au-TiO₂ after 24 hours long photocatalytic reduction of 10 ppm of Hg(II) in absence of chloride. Inset: magnified image in which larger and brighter Au NPs are circled in green. (d) Hg(II) concentration trends during photocatalytic reduction of 10 ppm of Hg(II) at pH 7.0 in presence (solid line) and absence (dashed line) of chlorides using 20Au-TiO₂.

NaCl was intentionally introduced in solution for two main reasons: i) chlorides are always present in every Hg polluted aqueous medium (ranging from fresh to marine waters): ii) it was reported by Wang et al.¹⁶ that with powdered TiO₂ photocatalysts the presence of Cl⁻ is detrimental in terms of Hg(II) reduction capability, due to the formation of a variety of complexes, including HgCl⁺, HgCl₃⁻ and HgCl₄²⁻.

SEM images taken from a 20Au-TiO₂ specimen after an intentionally short reduction test (Fig. 3b) clearly revealed that Au NPs act as nucleation sites for the directional growth of calomel nanowires. This evidence, together with the observation that the diameters of calomel nanowires (as measured from Fig. 3a) are slightly lower than the diameters of Au NPs, would indicate that these wires exclusively grow starting from Au NPs.

It should be underlined that the formation of calomel nanowires is relevant as such because it strongly enhances the scavenging properties of the Au-TiO₂ photocatalyst (this is key especially when highly concentrated Hg solutions have to be treated). In the absence of NaCl, the formation of Hg₂Cl₂ filaments was not observed (Fig. 3c), and in these conditions the photocatalytic Hg reduction is significantly slower (Fig. 3d). We report in Fig. 3c the SEM image of sample 20Au-TiO₂ after the reduction tests carried out in the absence of chlorides: the presence of some larger and brighter metallic NPs, which were not present before the photocatalytic experiment (Fig. 1c), is clearly visible. EDS analysis revealed that these larger NPs are composed of Au and Hg with a variable atomic Hg-Au ratio, which ranges from ~ 0.8 to 1.8. These results are consistent with the formation of an amalgam between Hg(0) and Au, and in this case the mechanism would probably involve the complete reduction of Hg(II) to Hg(0).

XRD patterns recorded prior and after the photocatalytic test carried out without chlorides (compare patterns a-d in Fig. 4) show a substantial loss of crystallinity of the Au NPs: the decrease in intensity of Au (200) reflection at ~ 44.6° is consistent with the suggested formation of Au-Hg alloy.^{50,51} As we will show later, this is also confirmed by XPS analysis. A partial loss of crystallinity was observed also in the XRD spectrum (Fig. 4b) recorded after the photoreduction test carried out in the presence of chlorides (i.e. with the formation of Hg₂Cl₂ filaments): therefore, the partial formation of Hg-Au amalgams may not be excluded even in this case; however, owing to the structure coverage caused by the calomel nanowires, we could not observe by SEM the formation of structures comparable to those in Fig. 3d (Hg-Au NPs).

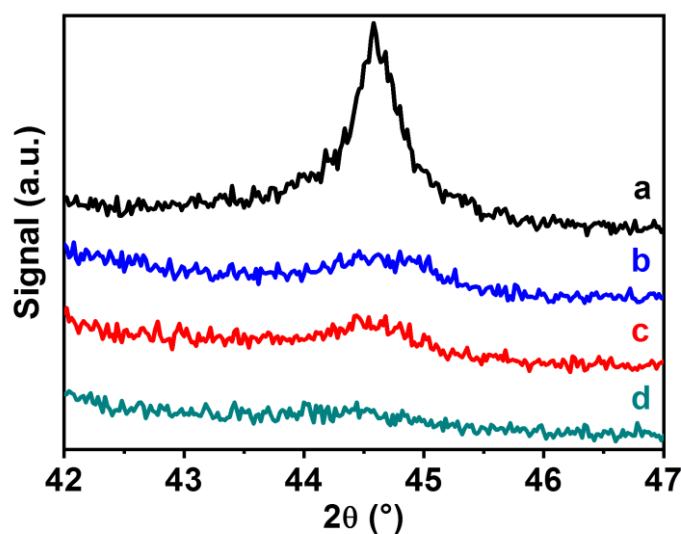


Fig. 4. Detail of Au (200) reflection in XRD spectra for 4 differently treated samples: (a) as-prepared 20Au-TiO₂; (b) 20Au-TiO₂ after photocatalytic reduction of 10 ppm of Hg(II) in presence of chloride; (c) the same material reported in (b) after PEC regeneration in KNO₃; (d) 20Au-TiO₂ after photocatalytic reduction of 10 ppm of Hg(II) in absence of chloride. Full XRD spectra are provided in Fig. S2.

The XPS spectra reported in Figs 5a-d and Fig. S3 further confirm the formation of calomel nanowires in the presence of chlorides, and the formation of Hg-Au alloy in the absence of chloride. The XPS analysis of 20Au-TiO₂ after photoreduction of Hg(II) in the presence of chlorides revealed two peaks at 101.05 eV and 105.10 eV which can be attributed to the Hg4f_{7/2} and Hg4f_{5/2} signals of Hg₂Cl₂.^{52,53} Instead, the formation of Hg-Au alloy (i.e. Hg(0)) in the absence of chlorides is supported by a shift and be the broadening of the Hg signals, which can fitted according to two doublets peaking at 98.90 and 102.79 eV, and 99.99 and 103.92 eV (Hg4f_{7/2} and Hg4f_{5/2}, respectively).^{53,54} The doublet nature and broadening of the Hg XPS signal reflects that Hg(0) is present with different chemical surroundings; such signal can e.g. be ascribed to the formation of Hg-Au alloy with various stoichiometric composition,⁵⁵ and to the presence of “free” Hg(0) adsorbed on TiO₂ NTs or at the Au NP surface.⁵⁴ As shown in Fig. S3, the Au4f XPS doublet for as-prepared 20Au-TiO₂ peaks at 83.10 eV and 86.70 eV, which corresponds well to data in the literature on Au deposited on TiO₂.⁴⁰ These signals however

seem not to shift with the formation of calomel or Hg-Au alloy; this results is also in line with data in the literature.⁵⁴

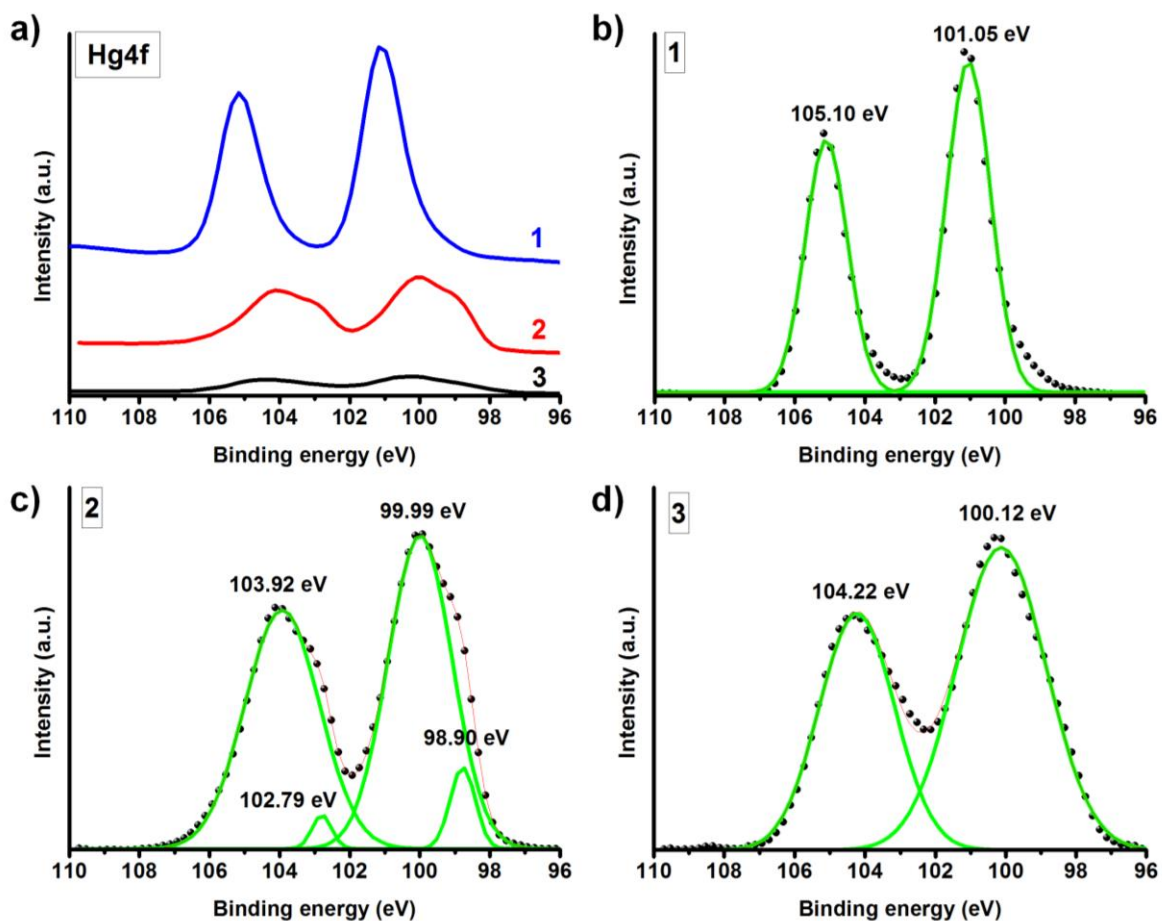


Fig. 5. (a) Comparison between Hg4f XPS spectra of (1) 20Au-TiO₂ after photocatalytic reduction of 10 ppm of Hg(II) in presence of chlorides, (2) 20Au-TiO₂ after photocatalytic reduction of 10 ppm of Hg(II) in absence of chlorides, (3) 20Au-TiO₂ after PEC regeneration. (b-d) Deconvolution of Hg4f signals for samples 1-3.

All the results so far reported can be rationalized as follows: i) Hg(II) \rightarrow Hg(0) proceeds stepwise with the intermediate formation of Hg(I); ii) in the presence of Cl⁻ the concentration of Hg(I) produced by photoreduction in close proximity of Au NPs is sufficiently high to grow Hg₂Cl₂ nanowires starting from such NPs; iii) in the absence of Cl⁻, the reduction further proceeds to Hg(0), i.e. with the formation of Hg-Au nano-amalgam; iv) a partial formation of Hg-Au amalgams cannot be excluded even in the presence of chlorides.

Apart from the presence of chlorides, the formation of calomel nanowires strongly depends on the amount of gold deposited on TiO₂ NTs and on the initial Hg concentration. In fact, the formation of such nanowires was neither observed on 1Au-TiO₂ (independently of the initial Hg concentration), nor on 20Au-TiO₂ for Hg concentration > 500 ppb (see Fig. S4a and S4b, respectively). Based on these results, we can infer that sufficiently big Au NPs, together with high Hg(II) concentrations, are fundamental to generate a sufficiently high Hg(I) local concentration to produce calomel nanowires. Apparently, the mechanism for such a directional and anisotropic growth of calomel nanowires roughly resembles the growth of carbon nanotubes starting from metal NPs,^{56,57} with the obvious difference that here we are working in the liquid phase rather than in the gas phase.

In any case, when the conditions are suitable for the growth of calomel nanowires, no Hg₂Cl₂ filaments produced from Au NPs inside TiO₂ nanotubes were observed, as well as from TiO₂. Additionally, when the conditions are not suitable for the growth of calomel nanowires, adsorption of Hg over TiO₂ surely occurs, as already reported in the literature.^{14,58,59} This evidence is only indirect (EDS resolution is not sufficient to locate Hg on TiO₂ rather than on Au), since the Au loading on TiO₂, cannot account for the scavenged Hg amounts.

Another investigated aspect was the possibility of reusing the Au-TiO₂ photocatalysts after a proper regeneration process. This investigation was conducted on 20Au-TiO₂ only, due to its superior performances at high Hg concentrations.

Since photo-reduced Hg is mainly loaded on Au NPs and on calomel nanowires bound to the Au NPs, the most rational way to efficiently reuse the photocatalyst is to selectively dissolve mercury, leaving behind Au NPs on TiO₂ NTs, that is, regenerating the original photocatalyst morphology and composition. In principle this process can be performed through an electrochemical oxidation of the Hg-loaded photocatalyst, in a similar way to the anodic

stripping determination of Hg on gold electrodes. This process would allow i) the regeneration of the photocatalyst (Hg-free Au NPs), and ii) the recovery of mercury in a small concentrated waste volume.

Therefore we investigated the feasibility of using an electrochemical dissolution in a KNO_3 100 mM media to regenerate the electrode. KNO_3 was chosen because of the high solubility of both mercuric and mercurous nitrates.⁶⁰ It should be underlined that, since TiO_2 is a semiconductor, it is mandatory to perform electrochemical dissolution under light illumination to produce the necessary charge carriers (as a matter of fact, any attempt to regenerate Au- TiO_2 catalysts applying up to 800 mV in the dark failed). In order to establish the regeneration potential to be applied to the Hg-loaded photocatalyst, cyclic voltammograms (CVs) were recorded in KNO_3 under illumination (Fig. 6a). One can observe the anodic region to start slightly above 0 mV (vs. Ag/AgCl). Moreover, as the stripping potential of Hg over gold electrodes is reported to fall on around 350-450 mV^{61,62} we decided to use 500 mV (a slightly more positive potential) as the regeneration potential.

From the current vs. time plot (Fig. 6b) recorded during the PEC regeneration it is possible to observe that a constant current value is reached after 120 min. The regeneration time was accordingly set to 120 min.

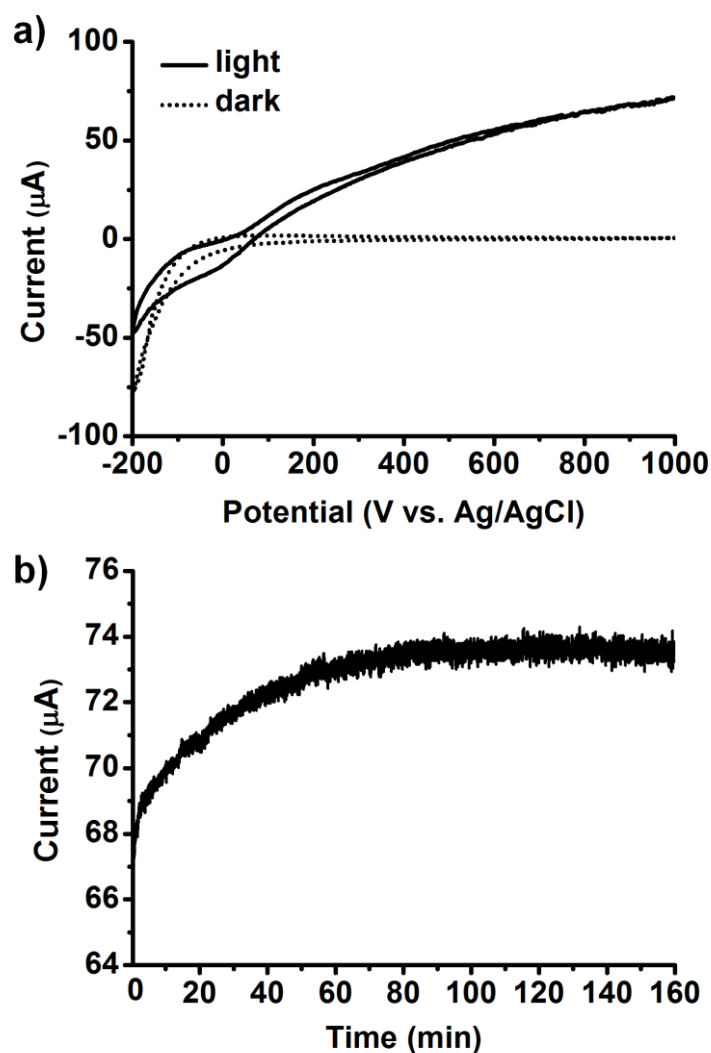


Fig. 6. (a) Cyclic voltammograms recorded using 20Au-TiO₂ in KNO₃ 100 mM with and without solar light irradiation; (b) chronoamperometric measurements recorded during 20Au-TiO₂ regeneration in 100mM KNO₃ solution applying 500 mV (vs. Ag/AgCl).

EDS analysis performed after PEC regeneration on different 20Au-TiO₂ samples revealed that the treatment was very successful: in the worst case only a ~ 0.14 Hg/Au atomic ratio was determined (please note that the Hg/Au ratios after Hg abatement were ~ 0.8 -1.8). Furthermore, ICP-MS analysis of the KNO₃ solution after regeneration revealed the presence of more than 80 % of the previously photocatalytically removed Hg(II). These results fit very well with the XPS analysis of 20Au-TiO₂ after PEC regeneration (Fig. 5): it is possible to observe a strong decrease of the XPS signals at 100.12 eV and 104.22 eV, which, as outlined above, is attributed to Hg(0).^{53,54}

As shown in Fig. 7, the regeneration process does not cause any modification of the Au NPs shape, and leads to a complete cleaning of the Au-TiO₂ structures from calomel nanowires. The only relevant difference between fresh and regenerated photocatalysts is reported in Fig. 4c, where it can be seen that the loss of crystallinity of Au NPs observed during the catalytic test is not recovered after regeneration.

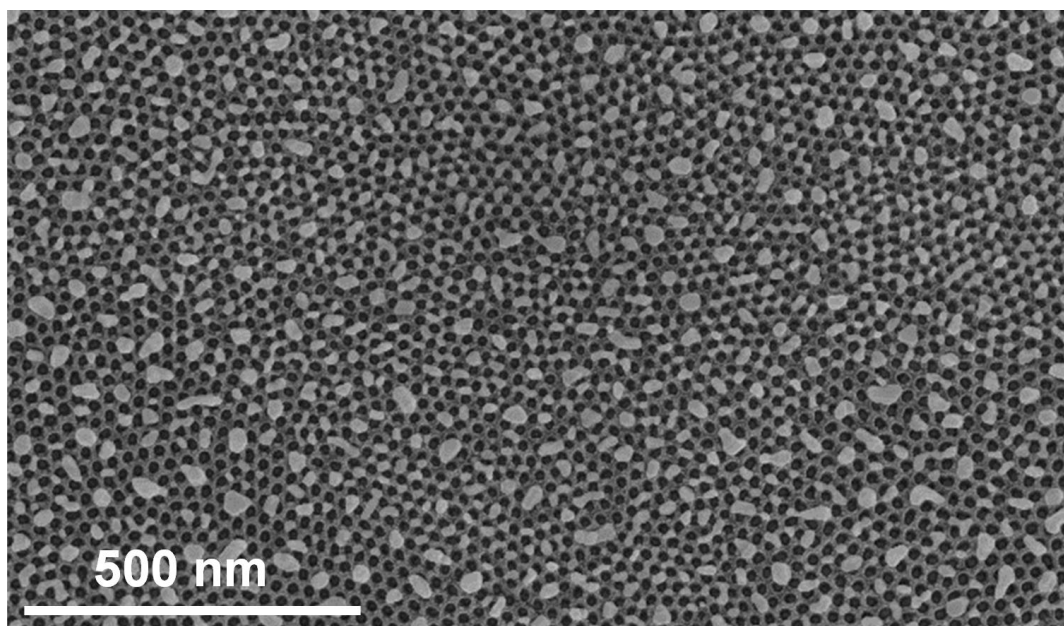


Fig. 7. SEM image of 20Au-TiO₂ after PEC regeneration procedure.

The abatement performances obtained for a freshly prepared 20Au-TiO₂ photocatalyst and for three subsequent recycling tests (a regeneration cycle was applied between each test) are schematically reported in Fig. 8. As it can be seen, the loss of activity is quite low even after 4 catalytic runs, indicating thus the effectiveness of the applied regeneration approach. These results are even more attractive if we consider that regeneration parameters were not optimized (this will be subject to further work).

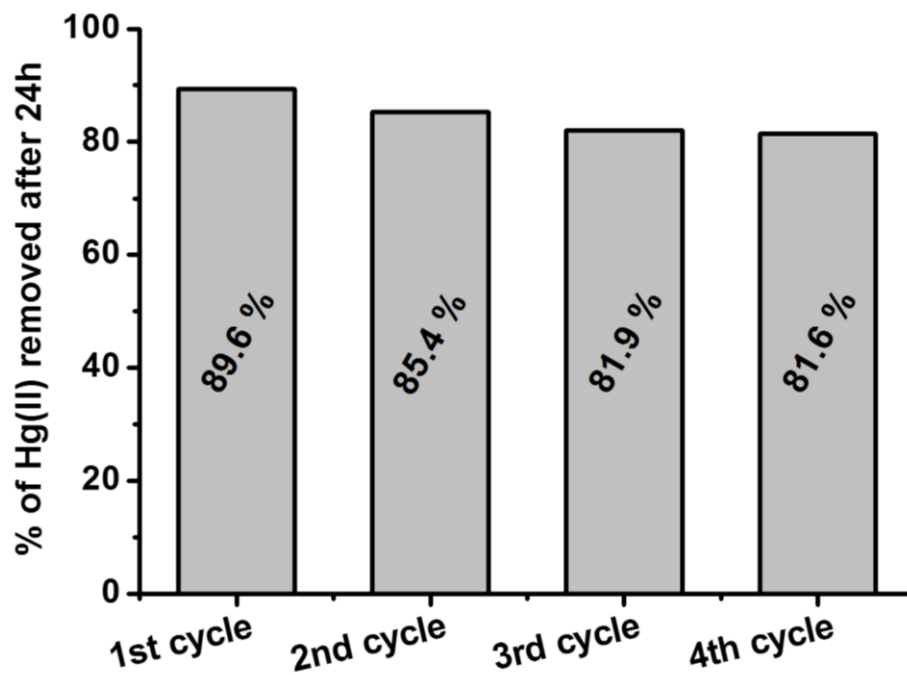


Fig. 8. Percentage of Hg(II) removed from 10 ppm Hg(II) chlorides-containing solutions after 24 hours long photocatalytic experiments carried out using 20Au-TiO₂ re-cycled up to 4 times

Conclusions

In this paper we have shown that Au-TiO₂ photocatalysts are able under sun light irradiation to efficiently photo-reduce Hg(II) to Hg(I) or Hg(0) and to accumulate these species. This functionality is enabled by the Au NPs at TiO₂ NT surface.

Two different mechanisms can be identified depending on the chloride concentration, Hg(II) concentration and Au NPs size. The first involves the partial reduction of Hg(II) to Hg(I) and, as a result, produce the massive formation of insoluble calomel nanowires that occurs when 20Au-TiO₂ is used to treat solution of quite high Hg(II) concentration levels and containing chlorides. A second mechanism involves the complete reduction of Hg(II) to Hg(0) and the formation of Hg-Au amalgam; this seems to occur whenever it is not possible to form insoluble Hg₂Cl₂.

Best results, in terms of Hg abatement, were obtained with the most Au-loaded photocatalyst (20Au-TiO₂). It is noteworthy that this photocatalyst has an intrinsic bimodal abatement behavior: at higher Hg concentrations the abatement proceeds through the formation of calomel wire (with attracting scavenging features), while the formation of Hg-Au amalgam is preferred at low Hg concentrations.

We also demonstrated the feasibility of an efficient regeneration of the photocatalyst by PEC anodic stripping, which additionally allows to recover the previously removed Hg(II) in a concentrated waste.

Acknowledgements

The authors would like to acknowledge ERC (340511), DFG and the DFG cluster of excellence EAM (EXC 315) for financial support. D.S. and S.R. gratefully acknowledge financial support from MIUR.

References

- 1 W. H. Schroeder and J. Munthe, Atmospheric mercury - An overview, *Atmos. Environ.*, 1998, **32**, 809–822.
- 2 M. Jaishankar, T. Tseten, N. Anbalagan, B. B. Mathew and K. N. Beeregowda, Toxicity, mechanism and health effects of some heavy metals, *Interdiscip. Toxicol.*, 2014, **7**, 60–72.
- 3 R. A. Bernhoft, Mercury Toxicity and Treatment: A Review of the Literature, *J. Environ. Public Health*, 2012, **2012**, 1–10.
- 4 K. M. Rice, E. M. Walker, M. Wu, C. Gillette and E. R. Blough, Environmental mercury and its toxic effects, *J. Prev. Med. Public Heal.*, 2014, **47**, 74–83.
- 5 R. P. Mason, J. R. Reinfelder and F. M. M. Morel, Bioaccumulation of mercury and methylmercury, *Water, Air, Soil Pollut.*, 1995, **80**, 915–921.
- 6 Q. Wang, D. Kim, D. D. Dionysiou, G. A. Sorial and D. Timberlake, Sources and remediation for mercury contamination in aquatic systems - A literature review, *Environ. Pollut.*, 2004, **131**, 323–336.
- 7 R. A. Lavoie, T. D. Jardine, M. M. Chumchal, K. A. Kidd and L. M. Campbell, Biomagnification of mercury in aquatic food webs: A worldwide meta-analysis, *Environ. Sci. Technol.*, 2013, **47**, 13385–13394.
- 8 A. E. Poste, D. C. G. Muir, S. J. Guildford and R. E. Hecky, Bioaccumulation and biomagnification of mercury in African lakes: The importance of trophic status, *Sci. Total Environ.*, 2015, **506–507**, 126–136.
- 9 EU, *Regulation (EU) 2017/852 of the European Parliament and of the Council of 17 May 2017 on mercury, and repealing Regulation (EC) No 1102/2008*, 2017.
- 10 J. G. Yu, B. Y. Yue, X. W. Wu, Q. Liu, F. P. Jiao, X. Y. Jiang and X. Q. Chen, Removal

- of mercury by adsorption: a review, *Environ. Sci. Pollut. Res.*, 2016, **23**, 5056–5076.
- 11 F. Fu and Q. Wang, Removal of heavy metal ions from wastewaters: A review, *J. Environ. Manage.*, 2011, **92**, 407–418.
 - 12 A. Sharma, A. Sharma and R. K. Arya, Removal of Mercury(II) from Aqueous Solution: A Review of Recent Work, *Sep. Sci. Technol.*, 2015, **50**, 1310–1320.
 - 13 M. A. Barakat, New trends in removing heavy metals from industrial wastewater, *Arab. J. Chem.*, 2011, **4**, 361–377.
 - 14 W. H. Lee, C. W. Lai and S. B. Abd Hamid, In Situ anodization of WO₃-decorated TiO₂ nanotube arrays for efficient mercury removal, *Materials (Basel)*, 2015, **8**, 5702–5714.
 - 15 M. A. Aguado, S. Cervera-March and J. Giménez, Continuous photocatalytic treatment of mercury(II) on titania powders. Kinetics and catalyst activity, *Chem. Eng. Sci.*, 1995, **50**, 1561–1569.
 - 16 X. Wang, S. O. Pehkonen and A. K. Ray, Photocatalytic reduction of Hg(II) on two commercial TiO₂ catalysts, *Electrochim. Acta*, 2004, **49**, 1435–1444.
 - 17 L. B. Khalil, M. W. Rophael and W. E. Mourad, The removal of the toxic Hg (II) salts from water by photocatalysis, *Appl. Catal. B Environ.*, 2002, **36**, 125–130.
 - 18 M. J. López-Muñoz, J. Aguado, A. Arencibia and R. Pascual, Mercury removal from aqueous solutions of HgCl₂ by heterogeneous photocatalysis with TiO₂, *Appl. Catal. B Environ.*, 2011, **104**, 220–228.
 - 19 G. G. Lenzi, C. V. B. Fávero, L. M. S. Colpini, H. Bernabe, M. L. Baesso, S. Specchia and O. A. A. Santos, Photocatalytic reduction of Hg(II) on TiO₂ and Ag/TiO₂ prepared by the sol-gel and impregnation methods, *Desalination*, 2011, **270**, 241–247.
 - 20 H. E. Byrne and D. W. Mazyck, Removal of trace level aqueous mercury by adsorption and photocatalysis on silica-titania composites, *J. Hazard. Mater.*, 2009, **170**, 915–919.

- 21 D. Sudha and P. Sivakumar, Review on the photocatalytic activity of various composite catalysts, *Chem. Eng. Process. Process Intensif.*, 2015, **97**, 112–133.
- 22 X. Chen, S. Shen, L. Guo and S. S. Mao, Semiconductor-based Photocatalytic Hydrogen Generation, *Chem. Rev.*, 2010, **110**, 6503–6570.
- 23 F. Opoku, K. K. Govender, C. G. C. E. van Sittert and P. P. Govender, Recent Progress in the Development of Semiconductor-Based Photocatalyst Materials for Applications in Photocatalytic Water Splitting and Degradation of Pollutants, *Adv. Sustain. Syst.*, 2017, **1**, 1700006.
- 24 J. Schneider, M. Matsuoka, M. Takeuchi, J. Zhang, Y. Horiuchi, M. Anpo and D. W. Bahnemann, Understanding TiO₂ photocatalysis: Mechanisms and materials, *Chem. Rev.*, 2014, **114**, 9919–9986.
- 25 P. Roy, S. Berger and P. Schmuki, TiO₂ Nanotubes: Synthesis and Applications, *Angew. Chemie Int. Ed.*, 2011, **50**, 2904–2939.
- 26 A. Fujishima, T. N. Rao and D. A. Tryk, Titanium dioxide photocatalysis, *J. Photochem. Photobiol. C Photochem. Rev.*, 2000, **1**, 1–21.
- 27 J. M. Macak, H. Tsuchiya, A. Ghicov, K. Yasuda, R. Hahn, S. Bauer and P. Schmuki, TiO₂ nanotubes: Self-organized electrochemical formation, properties and applications, *Curr. Opin. Solid State Mater. Sci.*, 2007, **11**, 3–18.
- 28 I. Paramasivam, H. Jha, N. Liu and P. Schmuki, A Review of Photocatalysis using Self-organized TiO₂ Nanotubes and Other Ordered Oxide Nanostructures, *Small*, 2012, **8**, 3073–3103.
- 29 M. Altomare, K. Lee, M. S. Killian, E. Selli and P. Schmuki, Ta-Doped TiO₂ Nanotubes for Enhanced Solar-Light Photoelectrochemical Water Splitting, *Chem. - A Eur. J.*, 2013, **19**, 5841–5844.

- 30 M. Altomare, M. Pozzi, M. Allieta, L. G. Bettini and E. Selli, H₂ and O₂ photocatalytic production on TiO₂ nanotube arrays: Effect of the anodization time on structural features and photoactivity, *Appl. Catal. B Environ.*, 2013, **136–137**, 81–88.
- 31 F. Riboni, N. T. Nguyen, S. So and P. Schmuki, Aligned metal oxide nanotube arrays: key-aspects of anodic TiO₂ nanotube formation and properties, *Nanoscale Horiz.*, 2016, **1**, 445–466.
- 32 C. Adán, J. Marugán, E. Sánchez, C. Pablos and R. van Grieken, Understanding the effect of morphology on the photocatalytic activity of TiO₂ nanotube array electrodes, *Electrochim. Acta*, 2016, **191**, 521–529.
- 33 M. Ge, C. Cao, J. Huang, S. Li, Z. Chen, K.-Q. Zhang, S. S. Al-Deyab and Y. Lai, A review of one-dimensional TiO₂ nanostructured materials for environmental and energy applications, *J. Mater. Chem. A*, 2016, **4**, 6772–6801.
- 34 M. Landmann, E. Rauls and W. G. Schmidt, The electronic structure and optical response of rutile, anatase and brookite TiO₂, *J. Phys. Condens. Matter*, 2012, **24**, 195503.
- 35 T. Luttrell, S. Halpegamage, J. Tao, A. Kramer, E. Sutter and M. Batzill, Why is anatase a better photocatalyst than rutile? - Model studies on epitaxial TiO₂ films, *Sci. Rep.*, 2014, **4**, 4043.
- 36 F. Forouzan, T. C. Richards and A. J. Bard, Photoinduced Reaction at TiO₂ Particles. Photodeposition from Ni^{II} Solutions with Oxalate, *J. Phys. Chem.*, 1996, **100**, 18123–18127.
- 37 S. Chen and L. W. Wang, Thermodynamic oxidation and reduction potentials of photocatalytic semiconductors in aqueous solution, *Chem. Mater.*, 2012, **24**, 3659–3666.
- 38 C. Schopf, A. Martín and D. Iacopino, Plasmonic detection of mercury via amalgam formation on surface-immobilized single Au nanorods, *Sci. Technol. Adv. Mater.*, 2017,

- 18**, 60–67.
- 39 M. Gärtner, V. Dremov, P. Müller and H. Kisch, Bandgap widening of titania through semiconductor support interactions, *ChemPhysChem*, 2005, **6**, 714–718.
- 40 J. E. Yoo, K. Lee, M. Altomare, E. Selli and P. Schmuki, Self-Organized Arrays of Single-Metal Catalyst Particles in TiO₂ Cavities: A Highly Efficient Photocatalytic System, *Angew. Chemie Int. Ed.*, 2013, **52**, 7514–7517.
- 41 Y. X. Zhang, B. Gao, G. Li Puma, A. K. Ray and H. C. Zeng, Self-Assembled Au/TiO₂/CNTs Ternary Nanocomposites for Photocatalytic Applications, *Sci. Adv. Mater.*, 2010, **2**, 503–513.
- 42 E. Ciceri, S. Recchia, C. Dossi, L. Yang and R. E. Sturgeon, Validation of an isotope dilution, ICP-MS method based on internal mass bias correction for the determination of trace concentrations of Hg in sediment cores, *Talanta*, 2008, **74**, 642–647.
- 43 D. Spanu, S. Recchia, S. Mohajernia, O. Tomanec, Š. Kment, R. Zboril, P. Schmuki and M. Altomare, Templated Dewetting–Alloying of NiCu Bilayers on TiO₂ Nanotubes Enables Efficient Noble-Metal-Free Photocatalytic H₂ Evolution, *ACS Catal.*, 2018, **8**, 5298–5305.
- 44 D. Spanu, S. Recchia, S. Mohajernia, P. Schmuki and M. Altomare, Site-selective Pt dewetting on WO₃-coated TiO₂ nanotube arrays: An electron transfer cascade-based H₂ evolution photocatalyst, *Appl. Catal. B Environ.*, 2018, **237**, 198–205.
- 45 M. Altomare, N. T. Nguyen and P. Schmuki, Templated dewetting: designing entirely self-organized platforms for photocatalysis, *Chem. Sci.*, 2016, **7**, 6865–6886.
- 46 J. Yoo, M. Altomare, M. Mokhtar, A. Alshehri, S. A. Al-Thabaiti, A. Mazare and P. Schmuki, Photocatalytic H₂ Generation Using Dewetted Pt-Decorated TiO₂ Nanotubes: Optimized Dewetting and Oxide Crystallization by a Multiple Annealing Process, *J.*

- Phys. Chem. C*, 2016, **120**, 15884–15892.
- 47 M. Altomare, N. T. Nguyen, S. Hejazi and P. Schmuki, A Cocatalytic Electron-Transfer Cascade Site-Selectively Placed on TiO₂ Nanotubes Yields Enhanced Photocatalytic H₂ Evolution, *Adv. Funct. Mater.*, 2018, **28**, 1704259.
- 48 G. Cha, P. Schmuki and M. Altomare, Anodic TiO₂ nanotube membranes: Site-selective Pt-activation and photocatalytic H₂ evolution, *Electrochim. Acta*, 2017, **258**, 302–310.
- 49 C. V Thompson, Solid-State Dewetting of Thin Films, *Annu. Rev. Mater. Res.*, 2012, **42**, 399–434.
- 50 S. F. L. Mertens, M. Gara, A. S. Sologubenko, J. Mayer, S. Szidat, K. W. Krämer, T. Jacob, D. J. Schiffrin and T. Wandlowski, Au@Hg nanoalloy formation through direct amalgamation: Structural, spectroscopic, and computational evidence for slow nanoscale diffusion, *Adv. Funct. Mater.*, 2011, **21**, 3259–3267.
- 51 T. Kobiela, B. Nowakowski and R. Dus, The influence of gas phase composition on the process of AuHg amalgam formation, *Appl. Surf. Sci. Appl. Surf. Sci.*, 2003, **206**, 78–89.
- 52 Y. V. Fedoseeva, A. S. Orekhov, G. N. Chekhova, V. O. Koroteev, M. A. Kanygin, B. V. Senkovskiy, A. Chuvilin, D. Pontiroli, M. Riccò, L. G. Bulusheva and A. V. Okotrub, Single-Walled Carbon Nanotube Reactor for Redox Transformation of Mercury Dichloride, *ACS Nano*, 2017, **11**, 8643–8649.
- 53 P. Bonnissel-Gissing, M. Alnot, J.-P. Lickes, J.-J. Ehrhardt and P. Behra, Modeling the Adsorption of Mercury(II) on (Hydr)oxides II: α -FeOOH (Goethite) and Amorphous Silica, *J. Colloid Interface Sci.*, 1999, **215**, 313–322.
- 54 T. Morris and G. Szulczewski, A Spectroscopic Ellipsometry, Surface Plasmon Resonance, and X-ray Photoelectron Spectroscopy Study of Hg Adsorption on Gold Surfaces, *Langmuir*, 2002, **18**, 2260–2264.

- 55 C. Ramasindarum, V. Balakrishnan, N. H. Abu Kasim and M. A. Yarmo, in *Characterization and Development of Biosystems and Biomaterials*, 2013, pp. 153–166.
- 56 J.-Y. Raty, F. Gygi and G. Galli, Growth of Carbon Nanotubes on Metal Nanoparticles: A Microscopic Mechanism from Ab Initio Molecular Dynamics Simulations, *Phys. Rev. Lett.*, 2005, **95**, 96103.
- 57 G. Hong, Y. Chen, P. Li and J. Zhang, Controlling the growth of single-walled carbon nanotubes on surfaces using metal and non-metal catalysts, *Carbon N. Y.*, 2012, **50**, 2067–2082.
- 58 B. Dou, V. Dupont, W. Pan and B. Chen, Removal of aqueous toxic Hg(II) by synthesized TiO₂ nanoparticles and TiO₂/montmorillonite, *Chem. Eng. J.*, 2011, **166**, 631–638.
- 59 Y. Li and C. Y. Wu, Role of moisture in adsorption, photocatalytic oxidation, and reemission of elemental mercury on a SiO₂-TiO₂ nanocomposite, *Environ. Sci. Technol.*, 2006, **40**, 6444–6448.
- 60 H. L. Clever, S. A. Johnson and M. E. Derrick, The Solubility of Mercury and Some Sparingly Soluble Mercury Salts in Water and Aqueous Electrolyte Solutions, *J. Phys. Chem. Ref. Data*, 1985, **14**, 631–680.
- 61 P. Salaün and C. M. G. Van Den Berg, Voltammetric detection of mercury and copper in seawater using a gold microwire electrode, *Anal. Chem.*, 2006, **78**, 5052–5060.
- 62 I. T. Somé, A. K. Sakira, D. Mertens, S. N. Ronkart and J.-M. Kauffmann, Determination of groundwater mercury (II) content using a disposable gold modified screen printed carbon electrode, *Talanta*, 2016, **152**, 335–340.